



OPEN

CONFERENCE
PROCEEDINGS

ISFM2014

.....

SUBJECT AREAS:

SOLAR CELLS

NANOSCALE MATERIALS

Received

2 October 2014

Accepted

16 December 2014

Published

23 March 2015

Correspondence and requests for materials should be addressed to LL. (lli@suda.edu.cn; liang.li0216@gmail.com)

Pt-free and efficient counter electrode with nanostructured CoNi_2S_4 for dye-sensitized solar cells

Zhiwei Shi, Kaimo Deng & Liang Li

College of Physics, Optoelectronics and Energy & Collaborative Innovation Center of Suzhou Nano Science and Technology, Soochow University, Suzhou 215006, P. R. China.

The counter electrode has a great influence on the performance of the dye-sensitized solar cells (DSSCs). The research and development of Pt-free counter electrode is becoming one of the hot areas in the field of DSSCs. Herein, we successfully synthesized a ternary metal sulfide (CoNi_2S_4) nanostructure on FTO substrate by hydrothermal method and investigated its application as counter electrode. The as-synthesized sample could exhibit better electrocatalytic property than that of Pt, and corresponding DSSCs have comparable conversion efficiency with typical Pt catalyzed cells. The easy synthesis, low cost and excellent electrocatalytic property may help the CoNi_2S_4 nanostructure stand out as an alternative counter electrode in DSSCs.

Dye sensitized solar cells have attracted extensive attentions in the past two decades as one of the most promising third generation solar cells, due to the excellent properties compared with silicon based solar cells such as low cost, relatively high efficiency, flexibility and easy fabrication^{1–3}. In general, a DSSC consists of an n-type semiconductor with a large band-gap (also named photoanode), dye molecules as sensitizer, a redox electrolyte and a counter electrode^{4–5}. By using newly synthesized ruthenium dyes and nanosized TiO_2 particles, Gratzel opened up a brand new era for the field of DSSCs and achieved an unprecedented efficiency over 12%⁶. However, this value is still lower than that of crystalline silicon based solar cells. The contemporary research and development of DSSCs mainly focus on the enhancement of efficiency and cost reduction. Great efforts have been devoted to developing efficient dye, employing photoanodes with different materials, structures and morphology and trying out other new kind of electrolyte. These developments have been reviewed in the recent articles⁷. On the other hand, the cost reduction can be generally realized by using cost-efficient materials and adopting low-temperature synthesis and processing^{8–9}. The platinum sputtered conducting glass usually serves as the counter electrode in a typical DSSC. It is known that Pt is extremely expensive and its reserve is quite limited. Meanwhile, the fabrication of Pt counter electrode needs heat treatment and it is unfavorable for the development of flexible plastic substrate. So there is an urgent need to explore alternative Pt-free materials with a cheaper price as the counter electrode in the large scale production of DSSCs.

As one of the most important part in DSSCs, the counter electrode acts as a catalyst by reducing the redox species after the electron injection so that the dye molecules can be regenerated. To fulfill this function, counter electrode materials should possess superior catalytic activity and chemical stability against the corrosive electrolyte in the DSSCs. As a traditional choice of counter electrode materials in DSSCs, Pt satisfies both the requirements thanks to its outstanding properties¹⁰. In fact, quite a few alternative materials, such as carbon materials^{11–13} and conducting polymers^{14–15}, have been used and investigated to replace Pt. In recent years, transition metal sulfides, such as NiS, CoS, WS and MoS_2 , have also found their application in DSSCs as counter electrodes^{16–18}. For example, Ho et. al.¹⁶ explored the performance of DSSCs using CoS as the counter electrode and the maximum conversion efficiency was nearly the same as that of the reference cell with a sputtered Pt counter electrode. The excellent performance of metal sulfide is largely related to the excellent electrocatalytic ability. In particular, transition metal sulfides have a variety of advantages over other counterparts such as easy synthesis, low cost and chemical stability, all of which render them attractive candidates as counter electrodes. However, it is noted that few ternary transition metal sulfides have been explored as counter electrodes in DSSCs^{19,20}. Ternary transition metal sulfides usually have a high electronic conductivity and they are also expected to have rich redox reactions due to the existence of nickel and cobalt ions²¹. In this report, for the first time, we investigate the synthesis of CoNi_2S_4 nanoparticle film and its application as counter electrode in DSSCs.

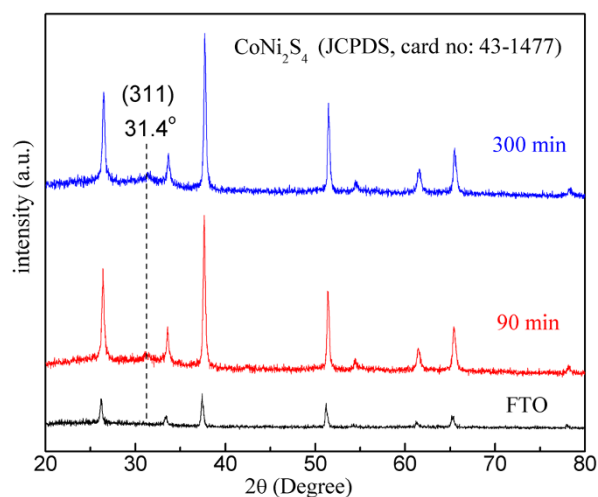


Figure 1 | XRD patterns of bare FTO substrate and samples after the synthesis of 90 min and 300 min.

Results

Fig. 1 shows the XRD patterns of the FTO substrates after hydrothermal reaction of 90 min and 300 min. It is noted that all the XRD patterns are dominated by the diffraction peaks from FTO substrates. Only one (311) peak at 31.4° is indexed to the phase (JCPDS, card no: 43-1477) of CoNi_2S_4 and no other impurity phase can be found. The XRD pattern of the sample underwent hydrothermal reaction of 20 min exhibits no obvious difference compared with that of the bare FTO substrate, indicating a small amount of products are formed on the substrate. To confirm the existence of CoNi_2S_4 , we performed X-ray photoelectron spectroscopy (XPS) experiments and the results are presented in Fig. 2. The XPS survey (Fig. 2a)

and high-resolution spectra of Ni 2p (Fig. 2b), Co 2p (Fig. 2c) and S 2p (Fig. 2d) match well with the reported data of CoNi_2S_4 ^{22–24}. The Ni 2p spectrum has two spin–orbit doublets characteristic of Ni^{2+} and Ni^{3+} , and two shake-up satellites (identified as “Sat”). Similarly, the Co 2p spectrum can also be considered by two spin–orbit doublets and two shake-up satellites. The S 2p spectrum shows two main peaks and one shake-up satellite. The peak at 162.4 eV is typical of metal–sulphur bonds, while the peak centered at 161.3 eV is attributed to sulphur ion in low coordination at the surface of samples.

The scanning electron microscopic (SEM) images of the FTO substrates with different reaction time are shown in Fig. 3. It can be seen that CoNi_2S_4 particles with an average diameter of 20 nm grow on the surface of the FTO substrate after the synthesis reaction of 20 min, leaving most surface areas of the crystalline grains uncovered (Fig. 3a, 3b). Due to the small amount of particles, the sample (denoted as NCS-20) still remains transparent as can also be found in the inset of Fig. 3a. The low loading of CoNi_2S_4 particles is responsible for the difficulty in detecting the X-ray diffraction peaks from the CoNi_2S_4 phase and taking the cross-section SEM image. After 90 min of the synthesis reaction, a continuous network with porous CoNi_2S_4 structure is formed on the substrate (Fig. 3c). The porous structure with a high surface area is beneficial for the catalytic reaction and the fast diffusion of I^-/I_3^- ions. The cross-section SEM image of the sample (NCS-90) shown in Fig. 4a indicates that the thin layer with a thickness of 500 nm is deposited evenly on the surface of the FTO substrate. For the sample with synthesis reaction of 300 min (NCS-300), the crystalline grains of the products become larger while the pore volume diminishes (Fig. 3d). Meanwhile, the increased reaction time results in more CoNi_2S_4 deposition on the substrate and an 800 nm thick film is obtained (Fig. 4b). To confirm the stoichiometry of these films, we mapped the elemental distribution of Ni, Co and S on the surface of samples, as shown in Fig. 5. Fig. 5a indicates the distribution of all three elements on the

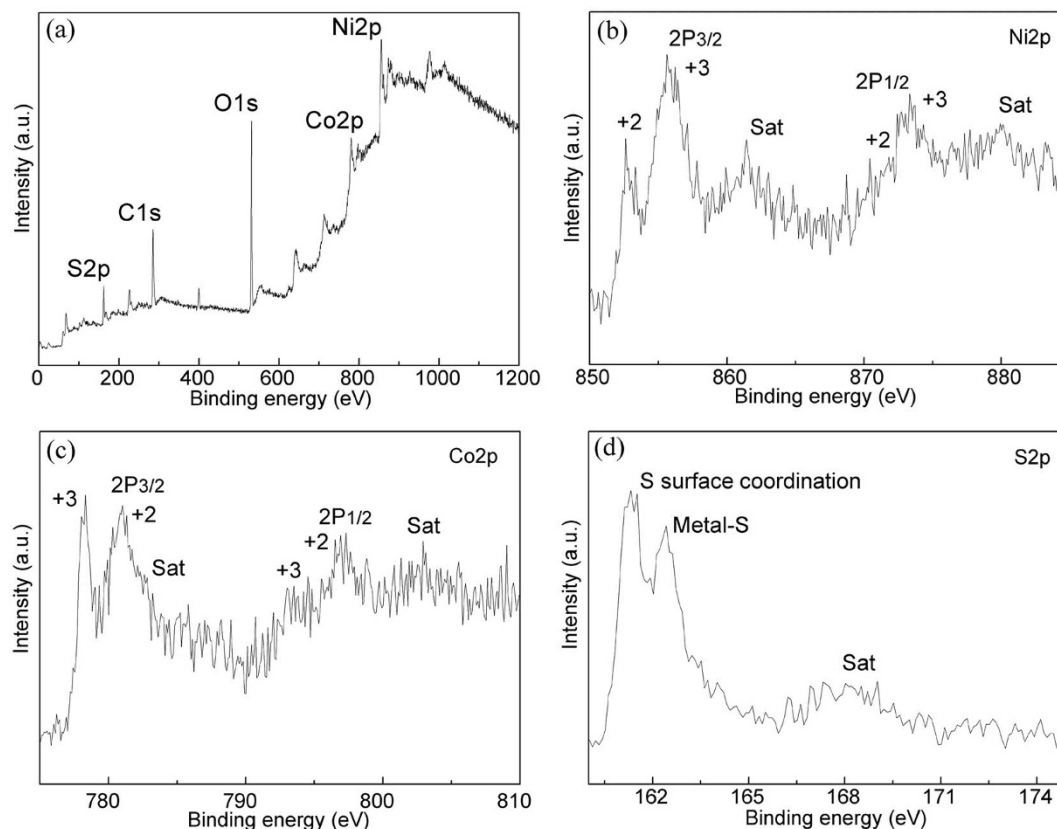


Figure 2 | (a) XPS survey spectra, (b) Ni 2p, (c) Co 2p, (d) S 2p XPS spectra of the products deposited on the surface of FTO substrate after 90 min reaction.

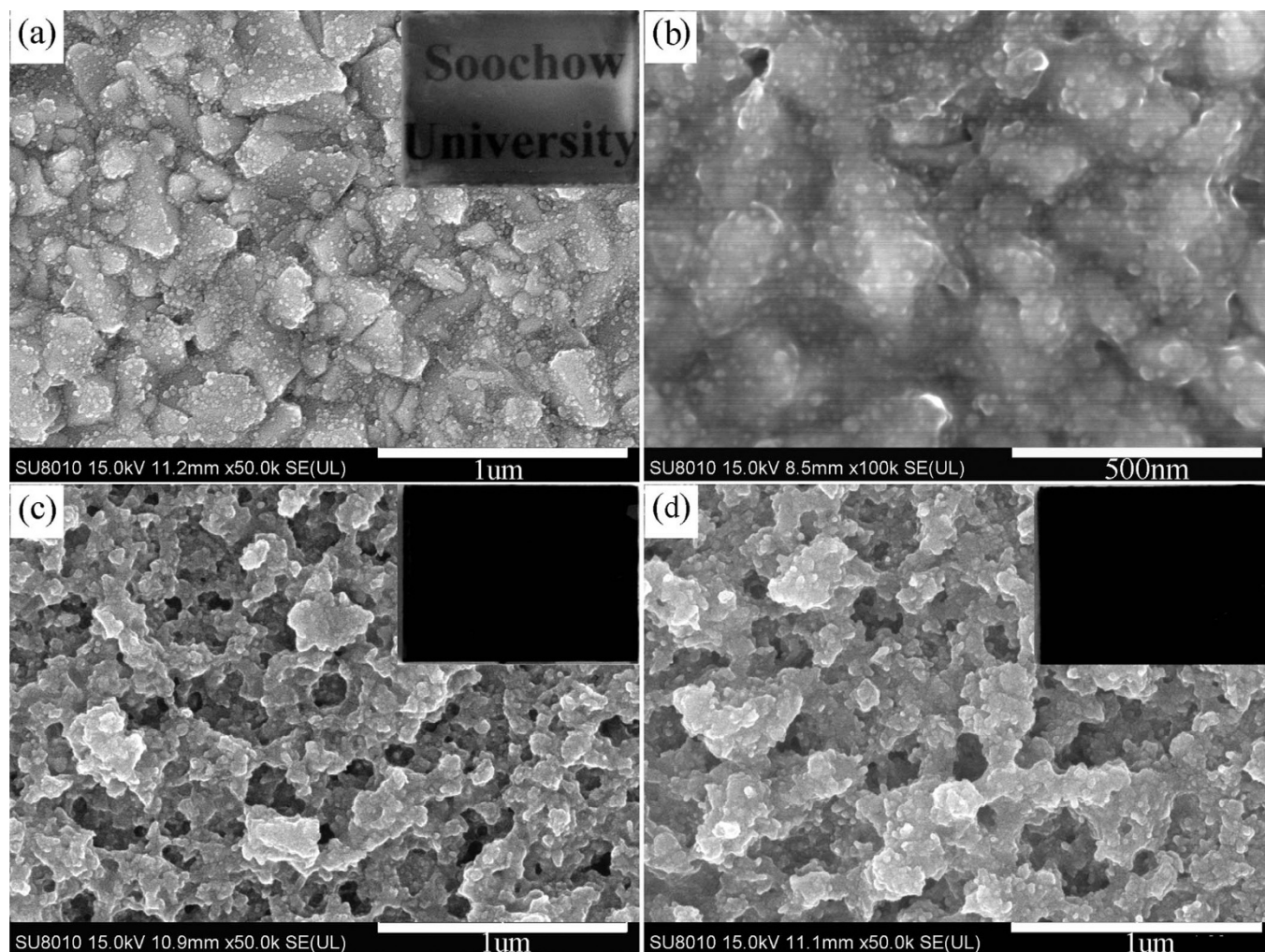


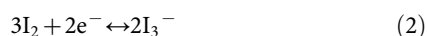
Figure 3 | SEM images the CoNi_2S_4 nanostructure synthesized under different reaction time: (a, b) 20 min, (c) 90 min and (d) 300 min. Inset shows the corresponding digital photos.

surface of scanned area, and the distribution of individual Ni, Co and S are also shown in Fig. 5b–5d, respectively. From these images, we can see that these elements are distributed uniformly. In addition, the relative ratio of elements is 8% : 16% : 30%, which is very close to a standard value (1 : 2 : 4) of CoNi_2S_4 .

To investigate the application of the CoNi_2S_4 as counter electrode, we studied the electrocatalytic properties of the counter electrode with the as-synthesized three types of CoNi_2S_4 nanostructures as well as the Pt film. The cyclic voltammetry (CV) curves of different counter electrodes under I^-/I_3^- electrochemical system using a three-electrode method are presented in Fig. 6. It can be found that all the CV curves, except that for the NCS-20, exhibit two pairs of redox peaks. The one at more negative potentials corresponds to the reaction²⁵:



and the other at more positive potentials relates to the reaction:



Since the counter electrode is the place where the reduction reaction of I_3^- in DSSCs is carried out, we will mainly focus on the oxidation and reduction of I^-/I_3^- at the more negative potentials. It is well accepted that the electrocatalytic ability of a counter electrode for I_3^- reduction in DSSCs can be reflected by the cathodic peak current at more negative potential. The higher the cathodic peak current

density is, the better the electrocatalytic ability will be²⁶. Meanwhile, another two conclusions can be made. First, the CV curve of NCS-20 is quite different from the other curves and there is no redox peaks at more negative potentials, indicating the poor electrocatalytic properties of the sample toward I_3^- reduction²⁷. This behavior is most likely related to the small amount of CoNi_2S_4 deposition. Second, the existence of the two pair redox peaks for the NCS-90 and NCS-300 sample shows that both of them have the electrocatalytic ability for reducing the triiodide ions. Their cathodic peak current densities are higher than those of Pt, and the NCS-300 has the highest value among all the counter electrodes. This implies that they have better electrocatalytic ability toward I^-/I_3^- redox couple than that of Pt.

To understand the charge transfer process at the interface between the electrolyte and the counter electrode, we measured the electrochemical impedance spectra (EIS) by using the symmetric sandwich-type configuration in order to eliminate the influence of the photoanode. The Nyquist plots for different counter electrodes are shown in Fig. 7. In each curve, there are two well-defined semicircles. The first semicircle at the high frequency region is related to the impedance of charge transfer process occurring at the counter electrode and electrolyte interface, while the other at lower frequency range can be assigned to the Nernst diffusion impedance within the electrolyte. Since a thin Surllyn film (60 μm) is used in the measurement, the Nernst diffusion impedance is insignificant and we will not discuss it in detail. Among all the counter electrodes, the NCS-20

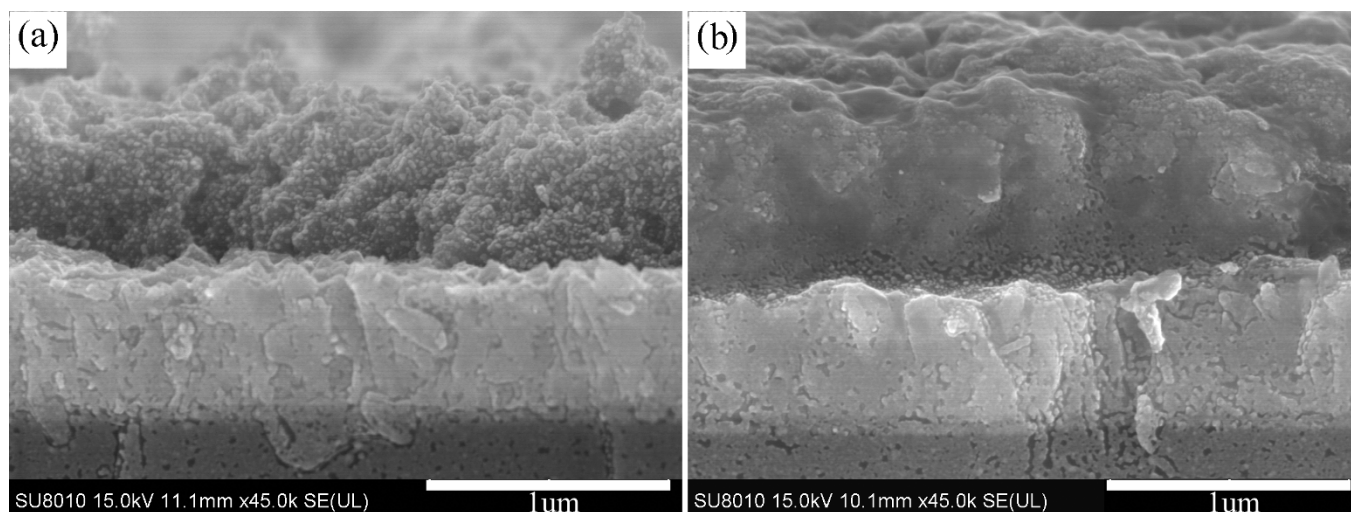


Figure 4 | Cross-section SEM image of CoNi_2S_4 nanostructure (a) NCS-90 and (b) NCS-300.

counter electrode has the largest semicircle in the Nyquist plot, suggesting that there is a large charge-transfer resistance (R_{ct})¹⁷, which is in accordance with the poor performance of reducing I_3^- ions in the CV measurement. The R_{ct} value of the NCS-90 is lower than that of the NCS-300. The Pt counter electrode has the lowest R_{ct} value. Besides the charge transfer impedance, the sheet resistance of the counter electrode (R_s) is another important parameter affecting the performance of counter electrode and it can also be obtained from EIS. We found that the NCS-90 has the lowest sheet resistance and the other counter electrodes have similar values. This demonstrates that CoNi_2S_4 has a prominent conductivity. Due to the increased thickness of the deposited film, the sheet resistance of the NCS-300 is larger than that of the NCS-90. Based on the above results, the NCS-90 has the best catalytic capability and the lowest R_{ct} , which is due to its proper film thickness. If the thickness is very small (NCS-20), the low amounts of nanoparticles cannot provide enough catalysis sites for chemical reaction, and if the thickness very large (NCS-300), the I^-/I_3^- solution cannot penetrate pores located in films and thus the catalytic effect is also decreased.

The photocurrent density versus photovoltage (J-V) curves of the DSSCs based on different counter electrodes are depicted in Fig. 8. The photovoltaic parameters including the short circuit current density (J_{sc}), open circuit voltage (V_{oc}), FF and energy conversion efficiency (η) corresponding to the DSSCs are summarized in the inset. It can be found that DSSCs based on NCS-20 counter electrode shows a rather low FF as a result of its poor electrocatalytic property. As for the NCS-90 counter electrode, the J_{sc} and FF value of the DSSCs increases obviously, leading to enhanced conversion efficiency from 2.49% to 4.61%. Both the excellent electrocatalytic property and the low sheet resistance contribute to the enhanced conversion efficiency. However, the efficiency of NCS-300 counter electrode-based DSSCs decreases a lot, chiefly arising from the decreased J_{sc} . This can be blamed on the increased charge transfer resistance at the counter electrode as confirmed by the EIS analysis. In short, the NCS-90 counter electrode exhibits the best performance among the three different NSC nanostructures. Its conversion efficiency is comparable to that of the Pt counter electrode-based DSSCs. In spite of a less satisfactory electrocatalytic property of the Pt counter electrode, DSSCs using Pt as catalyst still possess the highest conversion efficiency among all the DSSCs in our study. It should be pointed out that the conversion efficiency of DSSCs in our study is less than that of typical DSSCs. This is primarily because the TiO_2 photoanode of the DSSCs is about 8 μm in thick and lacks the scattering layer and our concern is mainly focused on the counter electrode, giving less attention on the conversion efficiency.

Discussions

Due to the high conductivity and excellent electrocatalytic property, Pt is widely used in DSSCs as counter electrode. The record conversion efficiency of DSSCs is also obtained by employing Pt as the catalyst. However, its large-scale application has to face two serious questions. First, Pt is expensive in price and scarce in reserve. Second, the Pt counter electrode is usually fabricated by thermal decomposition of HPtCl_4 or sputtering technology. Both the high temperature heat-treatment and the sputtering process are not beneficial to reduce the cost. So it is quite necessary to use an alternative catalyst with comparable electrocatalytic ability and cheaper price. Our study shows that ternary sulfide nanostructures could possess a better electrocatalytic ability than Pt. DSSCs assembled with the ternary sulfide CoNi_2S_4 nanostructures (NiCoS-90) as counter electrode has a similar conversion efficiency compared with DSSCs using Pt counter electrode. It is particularly important that the metal sulfide counter electrodes are synthesized by a conventional hydrothermal method at a low temperature of 130°C and no further calcination is required to complete the reaction. In addition, the raw materials in the synthesis are inexpensive and have a rich storage in the earth. These distinct characteristics would make it possible for the application of

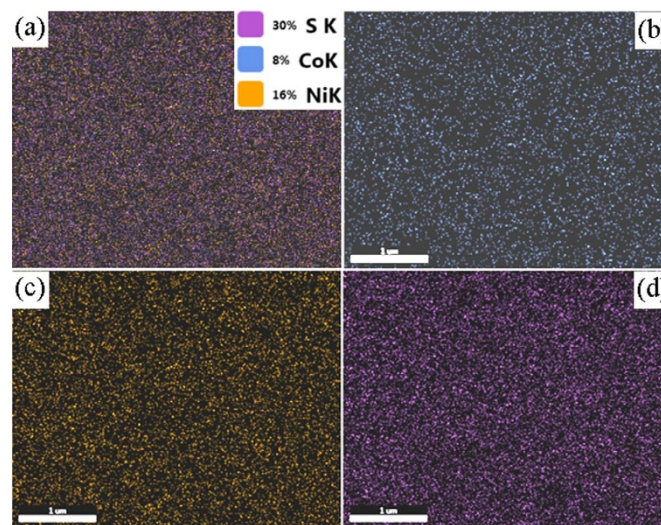


Figure 5 | Elemental mapping results of CoNi_2S_4 nanostructure film (NCS-90). (a) The whole element distribution on the surface and the inset is relative quantity, and (b–d) individual Co, Ni and S element distribution.

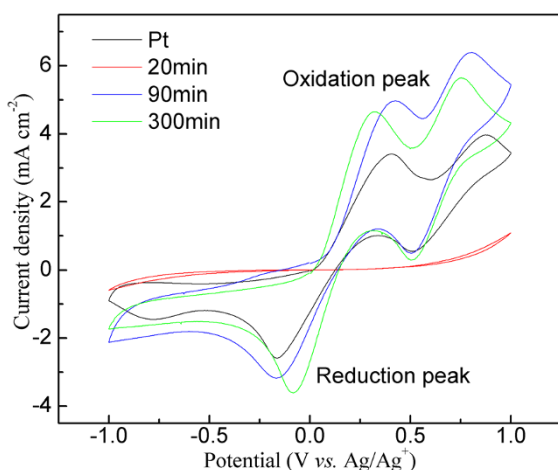


Figure 6 | CV curves of different counter electrodes.

CoNi₂S₄ nanostructures as counter electrode but not at the expense of conversion efficiency.

In summary, we have synthesized different CoNi₂S₄ nanostructures on FTO substrates with a conventional hydrothermal method at temperature as low as 130 °C and investigate their application as counter electrode in DSSCs. CV test shows that the CoNi₂S₄ nanostructures could exhibit better electrocatalytic property than Pt. The DSSCs with CoNi₂S₄ nanostructures as counter electrode shows comparable conversion efficiency compared with Pt catalyzed DSSCs. The excellent electrocatalytic properties, simple synthesis and low cost of the CoNi₂S₄ nanostructures may make the large-scale production of DSSCs become a more achievable goal.

Methods

Synthesis CoNi₂S₄ nanoparticles film. The CoNi₂S₄ nanoparticles films were synthesized via a one-step hydrothermal reaction. Briefly, 2 mmol Cobaltous acetate and 4 mmol Nickel acetate were dissolved in 30 ml deionized water, followed by the addition of 0.1 g Polyvinylpyrrolidone, 1 mmol NH₄F, and 2 mmol Urea. Then the mixture was transferred to a capped bottle with a FTO growth substrate facing down in the precursor at 130 °C for 20 min, 90 min, 300 min respectively. After reaction, the samples were rinsed with deionized water and dried in vacuum oven at 60 °C. It should be noted that we just obtained the nanosheet-like films when we modulated the relative amounts of NH₄F (2–10 mmol) and Urea (3–15 mmol), as shown in Fig. S1.

Fabrication of DSSC devices. A 20 nm-sized TiO₂ (P25, Degussa, Germany) layer (8 μm) was printed on FTO glass. When the obtained films sintered at 500 °C for 30 min were cooled to 90 °C, they were immersed in an ethanol solution containing 0.5 mM of N719 dye (cisbis(isothiocyanato) bis (2,2'-bipyridyl-4,4'-dicarboxylic acid) ruthenium(II)) (Solaronix) for 24 h, followed by rinsing in ethanol to remove

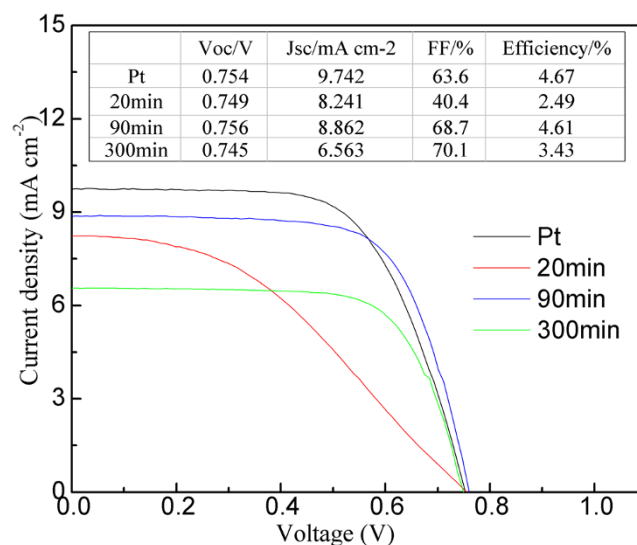
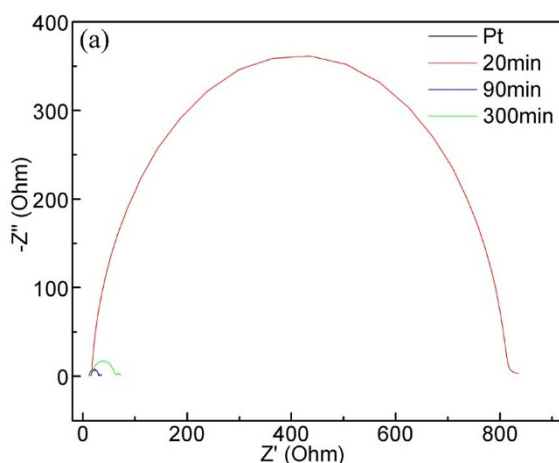


Figure 8 | Photocurrent density versus photovoltage curves of DSSCs based on different counter electrodes.

dye absorbed physically and drying in air. The Pt counter electrode was prepared by spin-coating 1 mM of chloroplatinic acid (H₂PtCl₆·6H₂O, Aldrich, 99.9%) in 2-propanol (Aldrich, 99.7%) onto a FTO substrate and then heating at 350 °C for 30 min. The as-prepared Pt film is composed of discontinuous nanoparticles with a diameter smaller than 20 nm (Fig. S2). The as-prepared CoNi₂S₄ nanoparticles films were used directly as counter electrodes. The dye-coated photoanodes were sealed against Pt or CoNi₂S₄ counter electrodes with hot melt plastic spacers (Solaronix, 60 μm thick). The electrolyte (0.1 M LiI, 0.03 M I₂, 0.5 M tetrabutylammonium iodide and 0.5 M 4-tert-butylpyridine in acetonitrile) was introduced into the gap between two electrodes by a syringe. The active area of DSSCs was 0.25 cm².

Materials characterization. The morphology of our samples was characterized by field-emission scanning electron microscope (FESEM, Hitachi SU8010) with an elemental mapping apparatus. The phase of the products was checked by the X-ray diffractometer (XRD, D/MAX-III-B-40KV, Cu Kα radiation; λ = 0.15418 nm). The composition was measured by X-ray photoelectron spectroscopy (XPS, ESCALAB 250Xi, Thermo Scientific).

Device measurements. The photovoltaic test (J-V) were performed using a Keithley 2400 source meter under simulated AM 1.5G illumination (100 mW cm⁻²) provided by a solar light simulator (Newport, 94043A). Cyclic voltammetry (CV) and the electrochemical impedance spectroscopy (EIS) were recorded on an Autolab electrochemical workstation (PGSTAT 302N). CV was carried out in a three-electrode system with different counter electrodes as working electrodes, a Pt foil as counter electrode, and a Ag/Ag⁺ electrode as reference electrode at a scan rate of 50 mV s⁻¹. The electrodes were immersed into an anhydrous acetonitrile solution consisting of 0.1 M LiClO₄, 10 mM LiI, and 1 mM I₂. EIS was carried out with a symmetric cell assembled with two identical counter electrodes at open-circuit

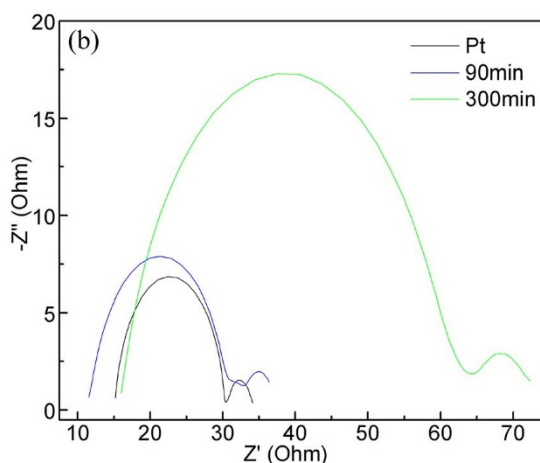


Figure 7 | EIS spectra of different counter electrodes.



voltage bias under dark condition at room temperature. The measured frequency ranged from 10 mHz to 1 MHz with an ac amplitude of 10 mV.

- O'Regan, B. & Grätzel, M. A low-cost, high-efficiency solar cell based on dye-sensitized colloidal TiO₂ films. *Nature* **353**, 737–740 (1991).
- Hardin, B. E., Snaith, H. J. & McGehee, M. D. The renaissance of dye-sensitized solar cells. *Nature Photon.* **6**, 162–169 (2012).
- Zhang, S. F., Yang, X. D., Numata, Y. & Han, L. Y. Highly efficient dye-sensitized solar cells: progress and future challenges. *Energy Environ. Sci.* **6**, 1443–1464 (2013).
- Zhang, Q. F., Dandeneau, C. S., Zhou, X. Y. & Cao, G. Z. ZnO nanostructures for dye-sensitized solar cells. *Adv. Mater.* **21**, 4087–4108 (2009).
- Yu, R., Lin, Q. F., Leung, S. F. & Fan, Z. Y. Nanomaterials and nanostructures for efficient light absorption and photovoltaics. *Nano Energy* **1**, 57–72 (2012).
- Yella, A. *et al.* Porphyrin-sensitized solar cells with cobalt (II/III)-based redox electrolyte exceed 12 percent efficiency. *Science* **334**, 629–634 (2011).
- Hagfeldt, A., Boschloo, G., Sun, L. C., Kloo, L. & Pettersson, H. Dye-sensitized solar cells. *Chem. Rev.* **110**, 6596–6663 (2010).
- Thomas, S. *et al.* A review on counter electrode materials in dye-sensitized solar cells. *J. Mater. Chem. A* **2**, 4474–4490 (2014).
- Yun, S., Hagfeldt, A. & Ma, T. L. Pt-free counter electrode for dye-sensitized solar cells with high efficiency. *Adv. Mater.* **36**, 6210–6237 (2014).
- Lee, Y. L. *et al.* A platinum counter electrode with high electrochemical activity and high transparency for dye-sensitized solar cells. *Electrochem. Commun.* **12**, 1662–1665 (2010).
- Murakami, T. N. & Grätzel, M. Counter electrodes for DSC: Application of functional materials as catalysts. *Inorg. Chim. Acta.* **361**, 572–580 (2008).
- Hong, W., Xu, Y., Lu, G., Li, C. & Shi, G. Transparent graphene/PEDOT-PSS composite films as counter electrodes of dye-sensitized solar cells. *Electrochem. Commun.* **10**, 1555–1558 (2008).
- Choi, H., Kim, H., Hwang, S., Choi, W. & Jeon, M. Sol. Fabrication and characterization of carbon-based counter electrodes prepared by electrophoretic deposition for dye-sensitized solar cells. *Energy Mater. Sol. Cells.* **95**, 323–325 (2011).
- Lee, K. S. *et al.* Dye-sensitized solar cells with Pt- and TCO-free counter electrodes. *Chem. Commun.* **46**, 4505–4507 (2010).
- Tang, Q., Cai, H., Yuan, S. & Wang, X. Counter electrodes from double-layered polyaniline nanostructures for dye-sensitized solar cell applications. *J. Mater. Chem. A* **1**, 317–323 (2013).
- Kung, C. W. *et al.* CoS acicular nanorod arrays for the counter electrode of an efficient dye-sensitized solar cell. *ACS Nano* **6**, 7016–7025 (2012).
- Sun, H. *et al.* Dye-sensitized solar cells with NiS counter electrodes electrodeposited by a potential reversal technique. *Energy Environ. Sci.* **4**, 2630–2637 (2011).
- Sun, X., Dou, J., Xie, F., Li, Y. & Wei, M. One-step preparation of mirror-like NiS nanosheets on ITO for the efficient counter electrode of dye-sensitized solar cells. *Chem. Commun.* **50**, 9869–9871 (2014).
- Lin, J. Y. & Chou, S. W. Highly transparent NiCo₂S₄ thin film as an effective catalyst toward triiodide reduction in dye-sensitized solar cells. *Electrochem. Commun.* **37**, 11–14 (2013).
- Banerjee, A. *et al.* Nickel cobalt sulfide nanoneedle array as an effective alternative to Pt as a counter electrode in dye sensitized solar cells. *RSC Advances* **4**, 8289–8294 (2014).
- Du, W. *et al.* Facile synthesis and superior electrochemical performances of CoNi₂S₄/graphene nanocomposite suitable for supercapacitor electrodes. *J. Mater. Chem. A* **2**, 9613–9619 (2014).
- Chen, H. *et al.* Highly conductive NiCo₂S₄ urchin-like nanostructures for high-rate pseudocapacitors. *Nanoscale* **5**, 8879–8883 (2013).
- Ohno, Y. Electronic structure of the misfit-layer compounds PbTiS₃ and SnNbS₃. *Phys. Rev. B* **44**, 1281–1291 (1991).
- Abraham, K. M. & Chaudhri, S. M. The lithium surface film in the Li/SO₂ cell. *J. Electrochem. Soc.* **133**, 1307–1311 (1986).
- Gong, F., Wang, H., Xu, X., Zhou, G. & Wang, Z. S. In situ growth of Co(0.85)Se and Ni(0.85)Se on conductive substrates as high-performance counter electrodes for dye-sensitized solar cells. *J. Am. Chem. Soc.* **134**, 10953–10958 (2012).
- Yoon, C. H., Vittal, R., Lee, J., Chae, W. S. & Kim, K. J. Enhanced performance of a dye-sensitized solar cell with an electrodeposited- platinum counter electrode. *Electrochim. Acta.* **53**, 2890–2896 (2008).
- Zhang, T., Chen, H., Su, C. & Kuang, D. A novel TCO- and Pt-free counter electrode for high efficiency dye-sensitized solar cells. *J. Mater. Chem. A* **1**, 1724–1730 (2013).

Acknowledgments

We acknowledge the support from the National Natural Science Foundation (51422206, 51372159, 11304217), 1000 Youth Talents Plan, Jiangsu Shuangchuang Plan, a Project Supported by Jiangsu Science and Technology Committee for Distinguished Young Scholars (BK20140009) and Funded by the Priority Academic Program Development of Jiangsu Higher Education Institutions (PAPD).

Author contributions

L.L. designed the experiment and analyzed results. Z.S. performed synthesis experiment and characterization. K.D. analyzed data and wrote the paper.

Additional information

Supplementary information accompanies this paper at <http://www.nature.com/scientificreports>

Competing financial interests: The authors declare no competing financial interests.

How to cite this article: Shi, Z., Deng, K. & Li, L. Pt-free and efficient counter electrode with nanostructured CoNi₂S₄ for dye-sensitized solar cells. *Sci. Rep.* **5**, 9317; DOI:10.1038/srep09317 (2015).



This work is licensed under a Creative Commons Attribution-NonCommercial-NoDerivs 4.0 International License. The images or other third party material in this article are included in the article's Creative Commons license, unless indicated otherwise in the credit line; if the material is not included under the Creative Commons license, users will need to obtain permission from the license holder in order to reproduce the material. To view a copy of this license, visit <http://creativecommons.org/licenses/by-nc-nd/4.0/>